Ocean Dynamics (2005) 55: 499–514
DOI 10.1007/s10236-005-0009-2

Carl Newell · Thomas Mullarkey · Mark Clyne

Radiation stress due to ocean waves and the resulting currents and set-up/set-down

Received: 1 February 2005 / Accepted: 25 May 2005 / Published online: 5 August 2005

Abstract The authors have developed a model to predict the radiation stresses in the coastal zone and to estimate currents and set-up/set-down of mean sea level. The values of radiation stress are calculated from velocity potential, which can be obtained by analytical means or from a finite element model of the elliptic extended mild slope equation depending on the complexity of the situation in question. The values of radiation stress are then input into a hydrodynamic model which gives the resulting set-up/set-down and currents caused by these stresses. The developed model includes convective acceleration and bottom friction. The radiation stress results of the model have been compared with analytical results and published values. Results for set-up/set-down and currents have been compared with published results for seven other similar models. The model has been compared with published results for set-up/set-down and currents created in the vicinity of a detached breakwater and also around a conical island. The results of the authors' model compare well with the analytical results, and published results for similar models.

Keywords Radiation stress · Currents · Set-up · Set-down · Wave potential

1 Introduction

The investigation and modelling of wave–current interaction (Doppler Effect) in the coastal zone is an ongoing area of research. Péchon et al (1997) examined seven models for calculating wave-driven currents, two of which also examine wave–current interaction. The authors of this paper are planning to examine wave–current interaction using a spatial finite element model. The two wave–current interaction models discussed by Péchon et al (1997) use finite difference calculation techniques. In order to develop a wave–current interaction model using spatial finite elements it was necessary to choose or develop a finite element wave model and a finite element hydrodynamic model. Some models of this type (such as ARTEMIS and TELEMAC) are available. The use of commercial software without access to the code was considered to be lacking with regards to adaptability so it was decided to use an elliptic extended mild slope wave model developed by Clyne and Mullarkey (2004) and to program the hydrodynamic model as part of the project. This paper deals with the validation of this wave-driven current model prior to investigation of wave–current interaction.

When an incident wave approaches a coastal area from deep water it experiences shoaling, which reduces the wavelength and increases the amplitude. If the wave approaches from an angle the decreasing depth causes refraction, with the wave crest gradually turning to align itself parallel to the contours of the seabed. Diffraction of waves around obstacles may also occur. When the wave reaches water that is sufficiently shallow, breaking occurs. Breaking waves on a beach cause a net momentum flux also known as radiation stress. The onshore component of this momentum flux is balanced by a pressure gradient in the opposite direction. The physical manifestation of this pressure gradient is a rise or fall of the mean sea level, known as set-up or set-down. The shear component of this momentum flux along with the pressure gradient creates second-order currents along and perpendicular to the coast. These currents are known as longshore and rip currents, respectively.

The authors' model includes non-linear convective terms as do some existing models. Older models such as Liu and Mei (1976) and Mei and Angelides (1976) ignored these effects for mathematical simplicity, how-

Responsible Editor: Paulo Salles

C. Newell (✉) · T. Mullarkey · M. Clyne
Department of Civil Engineering,
National University of Ireland Galway,
University Road, Galway, Ireland
E-mail: carl.newell@nuigalway.ie
Tel.: +353-91-52411
Fax: +353-91-750507

ever the incorporation of a non-linear friction term in the model means that the extra non-linearity brought about by the convective terms does not significantly alter the computational intensity of the model. The developed model uses an elliptic extended mild slope wave model, which is included in most similar models, such as ARTEMIS and MIKE 21. Many wave models, such as REF-DIF, use the parabolic approximation to the mild slope equation. From the experiences of Clyne and Mullarkey (2004), it was felt that an elliptic solution would better serve the needs of this project due to its enhanced behaviour in regions undergoing reflecting and diffracting waves.

2 Wave model

An elliptic extended mild slope wave model of Clyne and Mullarkey (2004) was chosen to model the waves. The model solves an elliptic equation in the domain. The elliptic solution for the mild slope wave equation of Berkhoff (1976) was extended to account for rapidly varying topography by Maa et al. (2002) and for energy dissipation by Booij (1981) is:

$$\nabla(a\nabla\phi) + \kappa^2 a\phi - \mathrm{i}\omega_0\gamma\phi + \left[f_1 g\nabla^2 h + f_2 g\kappa(\nabla h)^2\right]\phi = 0 \tag{1}$$

where

$a = cc_g$ (a product of the celerity and group velocity),
κ = local wave number calculated as the root of the dispersion relation,
$\nabla = \partial/\partial x\hat{i} + \partial/\partial y\hat{j}$ is a two-dimensional differential operator,
ϕ = the two-dimensional complex velocity potential without time,
γ = the energy dissipation factor,
ω_0 = the wave frequency,
g = acceleration due to gravity,
and the steep bottom coefficients f_1 and f_2 are:

$$f_1 = \frac{-4kh\cosh(kh) + \sinh(3kh) + \sinh(kh) + 8(kh)^2\sinh(kh)}{8\cosh^3(kh)[2kh + \sinh(2kh)]} - \frac{kh\tanh(kh)}{2\cosh^2(kh)} \tag{2}$$

$$f_2 = \frac{sech^2(kh)}{6[2kh + \sinh(2kh)]^3}\Big\{8(kh)^4 + 16(kh)^3\sinh(2kh) - 9\sinh^2(2kh)\cosh(2kh) + 12(kh)\left[1 + 2\sinh^4(kh)\right]\left[kh + \sinh(2kh)\right]\Big\} \tag{3}$$

The model uses a parabolic approximation to the mild slope equation as a boundary condition:

$$(a\kappa)^{\frac{1}{2}}\frac{\partial\phi}{\partial n} + \phi\frac{\partial}{\partial n}(a\kappa)^{\frac{1}{2}} - \mathrm{i}a^{\frac{1}{2}}\kappa^{\frac{3}{2}}\phi - \mathrm{i}P_2(a\kappa)^{-\frac{1}{2}}\frac{\partial}{\partial s}\left(a\frac{\partial\phi}{\partial s}\right) + P_2\frac{\omega_0\gamma}{(a\kappa)^{\frac{1}{2}}}\phi = 0 \tag{4}$$

where:

s is tangential to the boundary and perpendicular to n the outward normal,
P_2 = a constant multiplier originating from a binomial expansion of wave number terms.

The Clyne and Mullarkey (2004) wave model includes radiating boundary conditions to allowed reflected energy to leave the model. The energy dissipation term mentioned in Eq. 1 allows the use of complex breaking models; however, in this case it was chosen to use a linear breaking model in which the wave height is considered equal to 0.8 times the water depth in the surfzone. This is in line with both the ARTEMIS and STCPMVN mild-slope wave models examined by Péchon et al (1997).

Table 1 of Péchon et al (1997) summarises the properties of seven different wave models. The Clyne and Mullarkey (2004) model for this project uses mild slope wave equations, a breaking criterion in the surfsone of wave height/water depth = 0.8, and does not yet include wave–current interaction.

3 Radiation stress

The assumption of irrotational flow allows the velocity of water particles in the presence of a wave to be expressed as the gradient of a scalar, usually symbolised as ϕ, known as the velocity potential. The developed model uses calculated values of ϕ to calculate the various components of radiation stress S_{xx}, S_{yy}, S_{xy}, (S_{11}, S_{22}, S_{12}) where x is measured in the onshore direction and y is the longshore direction. The values of radiation stress are incorporated into the momentum equations, which along with the continuity equation are solved iteratively to obtain a solution for second-order currents and set-up/set-down. Mei (1994) develops a formula for the calculation of radiation stresses in the case of monochromatic waves:

$$S'_{ij} = \rho\left\{\frac{\overline{g\zeta'^2}}{2} + \int_{-h}^{\bar{\zeta}}\left(\frac{\partial}{\partial x_l}\int_{z}^{\bar{\zeta}}\overline{u'_l w'}\mathrm{d}z'\right)\mathrm{d}z - \int_{-h}^{\bar{\zeta}}\overline{w'^2}\mathrm{d}z\right\}\delta_{ij} + \rho\int_{-h}^{\bar{\zeta}}\overline{u'_i u'_j}\mathrm{d}z \tag{5}$$

where:

i, j, l = 1, 2 (where 1 and 2 are x and y, respectively)
u'_l, w' = horizontal and vertical wave particle velocity,

Table 1 Summary of wave models (from Péchon et al. - 1997)

	Equation	Breaking effect	Wave–current interaction
W1	Mild slope equations	Criterion in the surf-zone, wave height/water depth = 0.8	no
W2	Irrotational wave number, eikonal equation, wave action conservation	Energy dissipation given by Dally et al. (1985)	yes
W3	Parabolic mild slope equations, method of Kirby	Energy dissipation given by Battjes and Janssen (1978) modified for regular waves	no
W4	Irrotational wave number, eikonal equation, wave action conservation	Energy dissipation given by Battjes and Janssen (1978) modified for regular waves	no
W5	Irrotational wave number, eikonal equation, wave action conservation	Energy dissipation based on energy excess using a criterion for wave height	yes
W6	Mild slope equations	Criterion in the surf-zone, wave height/water depth = 0.8	no
W7	Hyperbolic time-dependent equations	Dispersion term	No

S'_{ij} = radiation stress,
ρ = density,
$\bar{\zeta}$ = set-up/set-down (measured above still water level),
ζ' = free surface (measured above still water level),
δ_{ij} = dirac delta,
h = depth.

An overbar indicates averaging over time.

In Eq. 5 the indices, i and j, on the left-hand side are the free indices. The free indices can appear only once on each term of the right-hand side and cannot be repeated. Where indices must be repeated the authors have used the dummy index l.

Equation 5 includes particle velocities and free surface height for the wave field. These values can be analytically calculated from the velocity potential, ϕ. The authors develop Eq. 5 into a form explicitly expressed in terms of ϕ (where ϕ is complex so $\phi = \phi_1 + i\phi_2$):

$$
\begin{aligned}
S''_{ij} = {} & \frac{\rho g \delta_{ij}}{4}\left(\left(\frac{-2\pi\phi_2}{Tg}\right)^2 + \left(\frac{2\pi\phi_1}{Tg}\right)^2\right) \\
& + \rho\delta_{ij}\left(\frac{\frac{\partial\phi_1}{\partial x_l}\frac{\partial\phi_1}{\partial x_l} + \phi_1\frac{\partial^2\phi_1}{\partial x_l\partial x_l} + \frac{\partial\phi_2}{\partial x_l}\frac{\partial\phi_2}{\partial x_l} + \phi_2\frac{\partial^2\phi_2}{\partial x_l\partial x_l}}{4\cosh^2(kh)}\right) \\
& \left[(h\cosh(2kh)) - \frac{\sinh(2kh)}{2k}\right] \\
& + \frac{\rho\delta_{ij}k^2\left(\phi_1^2 + \phi_2^2\right)}{4\cosh^2(kh)}\left[-h + \frac{\sinh(2kh)}{2k}\right] \\
& + \left(\frac{\frac{\partial\phi_1}{\partial x_i}\frac{\partial\phi_1}{\partial x_j} + \frac{\partial\phi_2}{\partial x_i}\frac{\partial\phi_2}{\partial x_j}}{4\cosh^2(kh)}\right)\left[h + \frac{\sinh(2kh)}{2k}\right]
\end{aligned} \tag{6}
$$

where:

$k = 2\pi/L$,
L = wavelength,
$i, j, l = 1, 2$
T = wave period.

Using Eq. 6 the radiation stress is calculated at each node on a finite element grid. The values of ϕ can be calculated analytically for simple cases such as waves at any angle approaching a beach with parallel contours. However, in the case of more complex models, analytical results are not always achievable. Where ϕ values are required for more complex models, the authors obtain these values from an elliptic extended mild-slope wave model described above. It should be noted that Eqs. 5 and 6 are suitable for the calculation of radiation stress for monochromatic waves only. Similar models, such as those discussed by Péchon et al (1997) also examine radiation stress only in the case of monochromatic waves.

4 Hydrodynamic behaviour

4.1 Two-dimensional model

In order to model the influence that radiation stress has on fluid behaviour in the coastal zone it is necessary to incorporate the radiation stress values into a hydrodynamic model. The chosen hydrodynamic model is suggested by Mei (1994) and Pinder and Gray (1977). The model is non-linear, vertically integrated and Cartesian. The governing hydrodynamic equations are the continuity Eq. 7 and two horizontal momentum Eq. 8:

$$
\frac{\partial\bar{\zeta}}{\partial t} + \frac{\partial\left(U_i\left(\bar{\zeta} + h\right)\right)}{\partial x_i} = 0 \tag{7}
$$

$$
\frac{\partial U_j}{\partial t} + U_i\frac{\partial U_j}{\partial x_i} + g\frac{\partial\bar{\zeta}}{\partial x_j} + \frac{\overline{\tau_j^B}}{\rho\left(\bar{\zeta} + h\right)} + \frac{1}{\rho\left(\bar{\zeta} + h\right)}\frac{\partial\left(S'_{ij} + S''_{ij}\right)}{\partial x_i} = 0 \tag{8}
$$

where:

i, j = 1, 2 (where 1 and 2 are x and y, respectively)
$\overline{\zeta}$ = set-up/set-down (measured above still water level),
U_i = vertically averaged velocities in x and y directions,
$\underline{g}$ = acceleration due to gravity,
$\overline{\tau_j^{\mathrm{B}}}$ = bottom stress.
S'_{ij} = radiation stress,
S''_{ij} = turbulent (Reynolds) stress,
ρ = density.

The momentum equations are integrated over the depth to produce depth averaged velocities. The Coriolis term is omitted due to the use of these equations in domains of limited horizontal extent. Equation 8 includes a turbulent (Reynolds) stress term. Mei (1994) ignores this term for mathematical simplicity as does the developed model. The wave-driven current models examined by Péchon et al (1997) include various different types of turbulence models; however, the paper concludes that further research is required to accurately model turbulence effects. The authors plan to research turbulent effects in more detail as suggested by Péchon et al (1997) before including any effect in the developed model.

The bed friction term is a non-linear quadratic equation including wave-driven velocity and wave orbital velocity. This equation is valid for application to currents in any direction in the two-dimensional hydrodynamic model regardless of the relative magnitudes of U and u'

$$\overline{\tau_j^{\mathrm{B}}} = \frac{f}{2}\rho\overline{|U+u'|\left(U_j+u'_j\right)} \tag{9}$$

where:

j = 1, 2 (where 1 and 2 are x and y, respectively),
U_j = vertically averaged velocities in x and y directions,
u'_j = wave particle velocities in x and y directions,
$\overline{\tau_j^{\mathrm{B}}}$ = bottom stress in x and y directions,
ρ = density.

The inclusion of this term and the convective acceleration term necessitates the use of an iterative solution scheme in time. Table 2 of Péchon et al (1997) summarises the properties of seven different wave-driven current models. The model developed for this project uses gradients of radiation stresses to drive currents, a quadratic law of wave-driven velocity + orbital velocity to model bottom friction and does not currently include a viscosity coefficient.

Equations 7 and 8 are solved using a finite element method. The authors' two-dimensional model uses linear triangular elements. Each dependent variable is first expanded within a typical element using shape functions and nodal values. These expanded forms are substituted into Eqs. 7 and 8 and the resulting equations are converted to matrix form using Galerkin's method. For example, the convective term in Eq. 8 can be expressed as follows for the two-dimensional model:

$$\int\int_A U_i^J \frac{\partial U_j^K}{\partial x} N^J N^K w^I \mathrm{d}x\, \mathrm{d}y \tag{10}$$

where:

I, J, K = 1, 2, 3 for linear triangular elements
i, j = 1, 2
w^I = weighting function (equal to the shape function in the case of the Galerkin method),
N^J & N^K = shape functions for a 2D triangle.

4.2 One-dimensional model

A simple one-dimensional model has also been created using line elements in the case of a beach with parallel contours; this allows for a computationally efficient calculation of currents and set-up/set-down for simple circumstances and also proves useful for debugging and examination of the more complicated two-dimensional model. Equations 7 and 8 can be rewritten as follows in a one-dimensional form:

$$\frac{\partial\overline{\zeta}}{\partial t} + \frac{\partial\left(U_1\left(\overline{\zeta}+h\right)\right)}{\partial x} = 0 \tag{11}$$

$$\frac{\partial U_1}{\partial t} + U_1\frac{1}{\partial x} + g\frac{\partial\overline{\zeta}}{\partial x} + \frac{\overline{\tau_1^{\mathrm{B}}}}{\rho\left(\overline{\zeta}+h\right)} + \frac{1}{\rho\left(\overline{\zeta}+h\right)}\frac{\partial\left(S'_{11}+S''_{11}\right)}{\partial x} = 0 \tag{12}$$

$$\frac{\partial U_2}{\partial t} + U_1\frac{2}{\partial x} + \frac{\overline{\tau_2^{\mathrm{B}}}}{\rho\left(\overline{\zeta}+h\right)} + \frac{1}{\rho\left(\overline{\zeta}+h\right)}\frac{\partial\left(S'_{12}+S''_{12}\right)}{\partial x} = 0 \tag{13}$$

In Eq. 12 the derivative of S_{11} in the onshore (x) direction governs set-up/set-down because at steady state U_1 is equal to zero. The first two terms in Eq. 13 are zero at steady state, therefore the derivative of S_{12} in the onshore (x) direction governs the longshore current and is balanced by the bottom friction term. Without a bottom friction term the solution would never converge to steady state as the longshore current would increase ad infinitum.

The resulting equations are converted to matrix form using Galerkin's method as in the case of the two-dimensional model. For example, the convective term of Eq. 12 above becomes the following in the case of the one-dimensional model:

$$\int_L U_1^J U_1^K \frac{\partial L^K}{\partial x} L^J w^I \, \mathrm{d}S \tag{14}$$

where:

I, J, K = 1, 2 for linear elements
i, j = 1, 2

Table 2 Summary of current models (from Péchon et al. 1997)

	Driving force	Viscosity coefficient	Bottom friction
C1	Energy dissipation formulation, three-dimensional	Constant + wave energy dissipation	Quadratic law of WDV
C2	Gradients of radiation stresses, vertical-horizontal correlation	Kinetic energy equation	Quadratic law of WDV + orbital velocity
C3	Gradients of radiation stresses	Constant	Quadratic law of WDV
C4	Energy dissipation formulation	Energy dispersion of wave and bottom friction	Quadratic law of WDV
C5	Energy dissipation formulation	Energy dispersion of wave and bottom friction	Quadratic law of WDV
C6	Gradients of radiation stresses	Constant	Quadratic law of WDV + orbital velocity
C7	Without the assumption of progressive waves	Kinetic energy equation	Quadratic law of WDV

w^I = weighting function, (equal to the shape function in the case of the Galerkin method),
L^J & L^K = shape functions for a 1D.

4.3 Time integration

Equations 7 and 8 for two dimensions or 11, 12 and 13 for one dimension are discretised. The time derivatives are solved using an implicit finite difference scheme over a time step Δt resulting in the following equations, after Pinder and Gray (1977):

$$[KI]\{\bar{\zeta}\}_{t+\Delta t} = [KI]\{\bar{\zeta}\}_t + \frac{1}{2}\Delta t\left\{E_{\bar{\zeta}}\right\}_{t+\Delta t} + \frac{1}{2}\Delta t\left\{E_{\bar{\zeta}}\right\}_t = \left\{R_{\bar{\zeta}}\right\} \tag{15}$$

$$[KI]\{U_i\}_{t+\Delta t} = [KI]\{U_i\}_t + \frac{1}{2}\Delta t\{E_{U_i}\}_{t+\Delta t} + \frac{1}{2}\Delta t\{E_{U_i}\}_t = \{R_{U_i}\} \tag{16}$$

where:

$[KI]$ = coefficient matrix from the partial time derivatives in Eqs. (7), 8 or 11, 12 and 13
$\{E\}$ = remaining terms from Eqs. 7, 8 or 11, 12 and 13
$\{R\}$ = residual.

From the known solution at t, estimates are made for $\bar{\zeta}$, U_1, and U_2, at $t + \Delta t$. These estimates are used to approximate $\left\{E_{\bar{\zeta}}\right\}_{t+\Delta t}$, $\{E_{U_1}\}_{t+\Delta t}$ and $\{E_{U_2}\}_{t+\Delta t}$, and thus completely determine the right-hand sides of Eqs. 15 and 16. Through iteration, more accurate estimates of the right-hand sides of Eqs. 15 and 16 are obtained until convergence of the finite element solution is achieved. After a converged finite element solution is obtained, calculation may proceed to the next time step until a steady state solution of set-up/set-down and current is reached. Instead of integration to steady state the time derivative could be eliminated, the governing equations would however continue to be non-linear. An iterative solution such as the Newton-Raphson method would have to be used instead. It was felt that this would not significantly increase the computational efficiency as both systems involve iteration.

5 Model results

The authors' model is run for a series of different circumstances. The wave model is initially compared with the results obtained from various wave models by Péchon et al (1997). Next the accuracy of the radiation stress term is examined. The model is then run for a one-dimensional mesh for the simple case of a wave approaching a beach with parallel contours. Finally the full model incorporating radiation stress and hydrodynamic effects is run for some more complex cases, including a wave approaching a detached breakwater on a beach with parallel contours and also a wave approaching the shore of a conical island.

5.1 Results (1)–Wave model

The Clyne and Mullarkey (2004) elliptic extended mild slope wave model has already been shown to compare favourably with analytical and numerical results for various systems in Clyne and Mullarkey (2003) and (2004). The wave model was run by the authors of this paper to obtain velocity potential values for the system modelled by Péchon et al (1997).

The system in question consists of a wave modelling tank 30 m by 30 m with a bed profile that starts with a 4.4 m section with a uniform depth of 0.33 m followed by a slope of 1:50 from the 0.33 m depth to the shoreline. The model also consists of an emerged plane beach with a slope of 1:20 to a height of 0.066 m above the still water level. A half-detached breakwater of 0.87 m width, 6.66 m long was built parallel to the beach at a distance of 10 m from the shoreline. Figure 1 shows the breaker lines obtained by the seven models tested by Péchon et al (1997) and the breaker line obtained using the Clyne and Mullarkey (2004) wave model. The modelled wave is a uniform wave with a period of 1.7 s and a wave height of 0.075 m.

The breaker line compares very favourably with those calculated by the other models and with the laboratory measured breaker line. There is some waviness apparent in the solution. This is due to some numerical noise that is evident in the model. A smoothening scheme has been

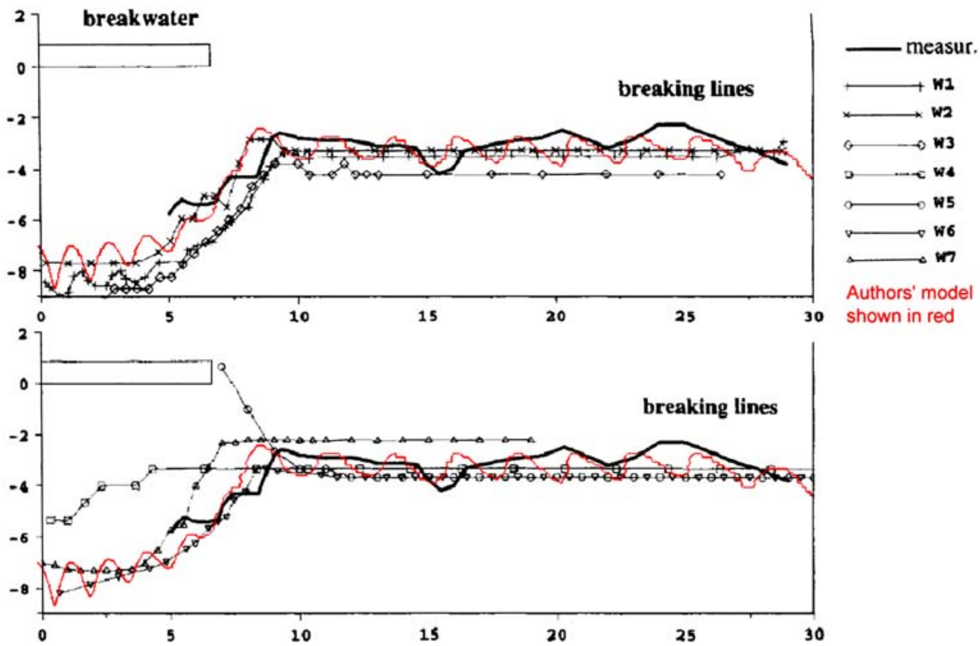

Fig. 1 Breaking lines for different wave models (from Péchon et al. 1997)

developed to alleviate this issue; however, it is not employed here in order to protect the integrity of the reflected portion of the diffracted wave that progresses behind the breakwater.

A cross-section of the wave heights perpendicular to the beach is shown in (Fig. 2). The cross-section is at a horizontal distance of 10 m from the breakwater side of the wave tank. This shows good comparison between the results of the Clyne and Mullarkey (2004) model and those of the other wave models.

5.2 Results (2a)–Radiation stress compared to Mei (1994) solution

The section of the model that calculates radiation stress is initially examined independently to ensure its accuracy prior to incorporation into the hydrodynamic model. The radiation stress values calculated for the simple case of a progressive wave approaching at an angle to a beach with parallel contours is considered. The authors calculate the ϕ values analytically for this case and input them into the radiation stress equation developed. The resulting radiation stress values are then compared with an analytical solution presented by Mei (1994) after Longuet-Higgins and Stewart (1962, 1964):

$$S'_{ij} = \frac{\rho g A^2}{4}\left\{\frac{k_i k_j}{k^2}\left(1+\frac{2kh}{\sinh 2kh}\right)+\delta_{ij}\frac{2kh}{\sinh 2kh}\right\} \tag{17}$$

where:

A = amplitude
k_1 = k cosθ
k_2 = k sinθ
θ = direction of wave propagation with respect to the x axis k, h as before

In the remainder of the results section the subscripts i and j on the radiation stress terms are replaced by x and y.

Mei (1994) mentions that Eq. 17 is designed for constant depth, but can be used as a good first approximation in the case of a slowly varying sea bed, provided the values of A and k are interpolated for the relevant water depth. To ensure that like is compared

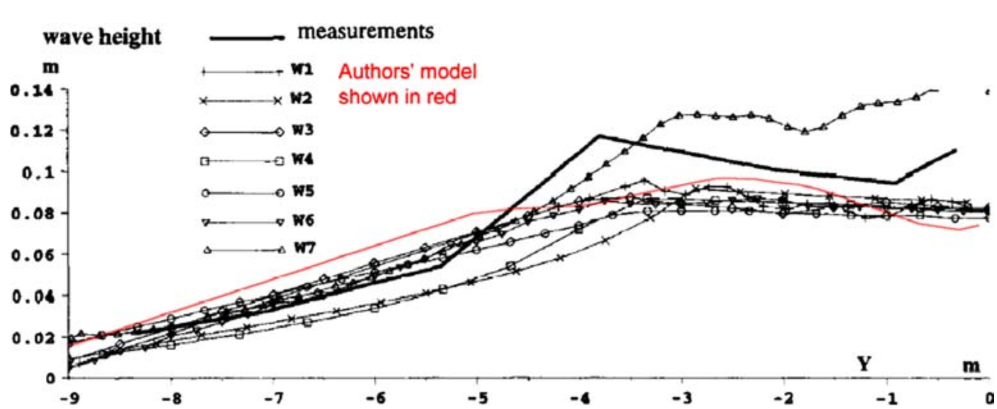

Fig. 2 Wave heights for different wave models (from Péchon et al. 1997)

with like the authors test their radiation stress model over a constant depth where Eq. 17 is most accurate. In this case, 2 metre amplitude wave with a 10 sec period travelling at 55° to a normal from the shore is chosen for comparison purposes and examined over a constant depth of 500 m where there is no shoaling. The results are shown in Figs. 3–5.The solution produced by Eq. 17 is constant through the entire length of the mesh, as expected for a constant deep water depth. In the case of the results produced by the authors' model, there is a slight

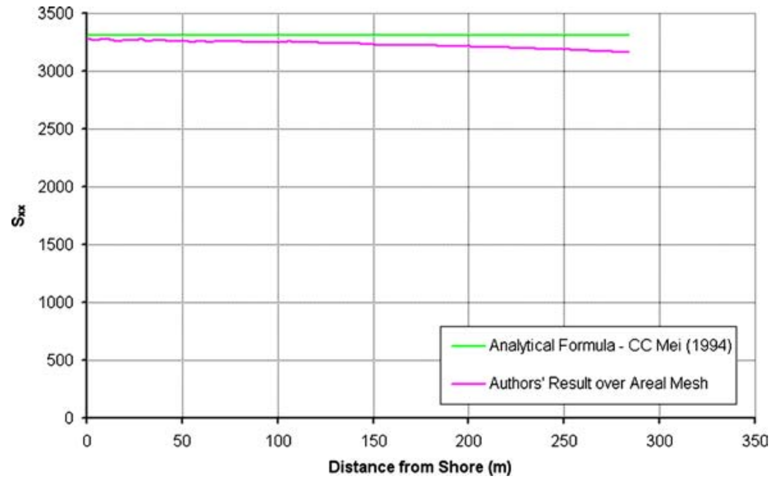

Fig. 3 S_{xx} (N/m) from the authors' radiation stress equation and from Mei's (1994) solution

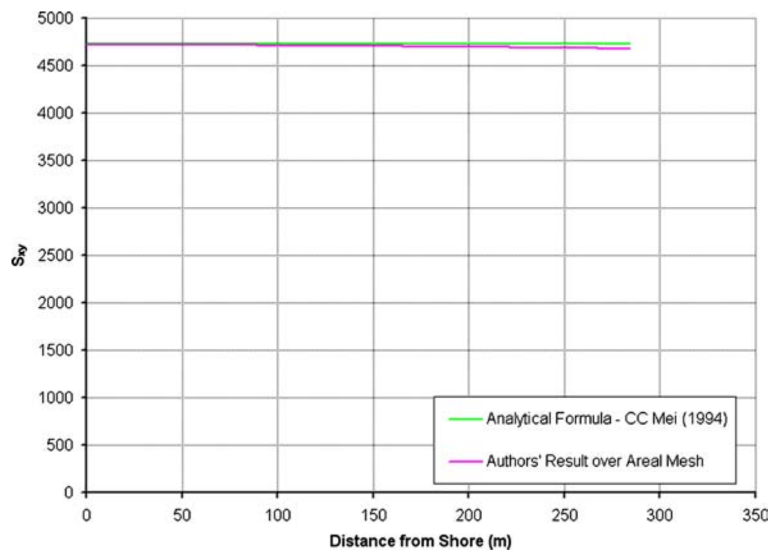

Fig. 4 S_{xy} (N/m) from the authors' radiation stress equation and from Mei's (1994) solution

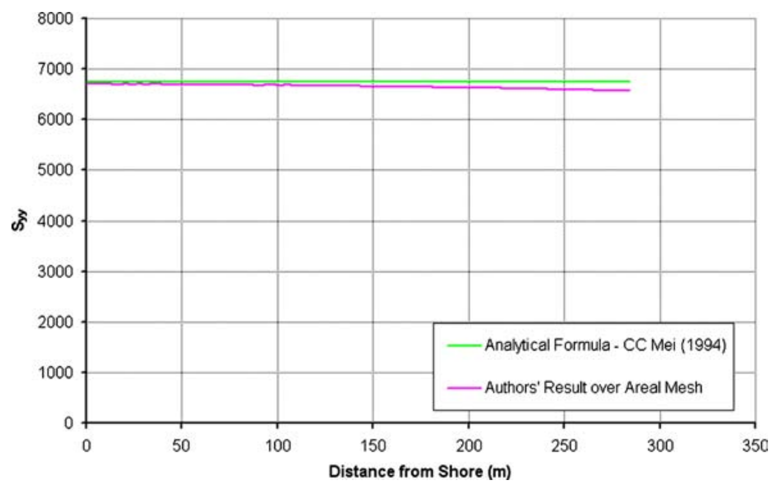

Fig. 5 S_{yy} (N/m) from the authors' radiation stress equation and from Mei's (1994) solution

Table 3 Percentage difference between authors' radiation stress equation and Eq. 15

Percentage difference (%)		
	Approx 0 m along mesh	Approx 300 m along mesh
S_{xx}	1.32	4.41
S_{xy}	0.09	0.99
S_{yy}	0.72	2.70

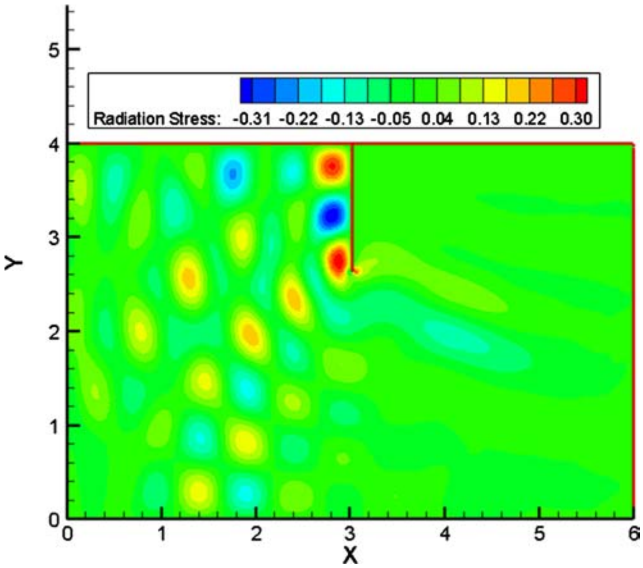

Fig. 6 S_{xy} from the authors' radiation stress model in N/m

change in the calculated values over the length of the entire mesh. This is due to the different element sizes over the mesh. The authors choose to gradually increase the element size as the distance increases away from the shore. This increases the computational efficiency of the model while not significantly impacting on its accuracy. The authors are only concerned with set-up/set-down and currents produced in and around the breaking zone, so at regions remote from this zone a dense mesh of elements would be inefficient. In the above example the triangular elements range from having a side length of approximately 1.2 m at one end of the mesh to having a side length of approximately 6 m at the opposite side of the mesh 360 m away. The percentage difference between the authors' results and those of Eq. 17 is summarized in Table 3.

It is worth noting that in the Figs. 3 – 5, the authors omit the value of radiation stress obtained from the edge element at each boundary of the domain in question. This element produces values with large errors due to the employed process of calculating elemental derivative values of ϕ by averaging those of the surrounding nodes. This does not pose problems for modelled results because in practice, the elements at the beach side boundary of the domain are very small and hence do not have a large effect on set-up/set-down or currents.

5.3 Results (2b)–Radiation stress compared to Watanabe and Maruyama's (1986) solution for a detached breakwater

Watanabe and Maruyama (1986) present plots of radiation stress values for the complex case of a detached breakwater on a sloping beach including wave breaking. Clyne and Mullarkey (2004) model the wave field generated for this problem. The ϕ values associated with the Clyne and Mullarkey (2004) model are used by the authors in the present paper. Except for one interesting exception the radiation stresses, calculated by the method outlined above, compare favourably with those

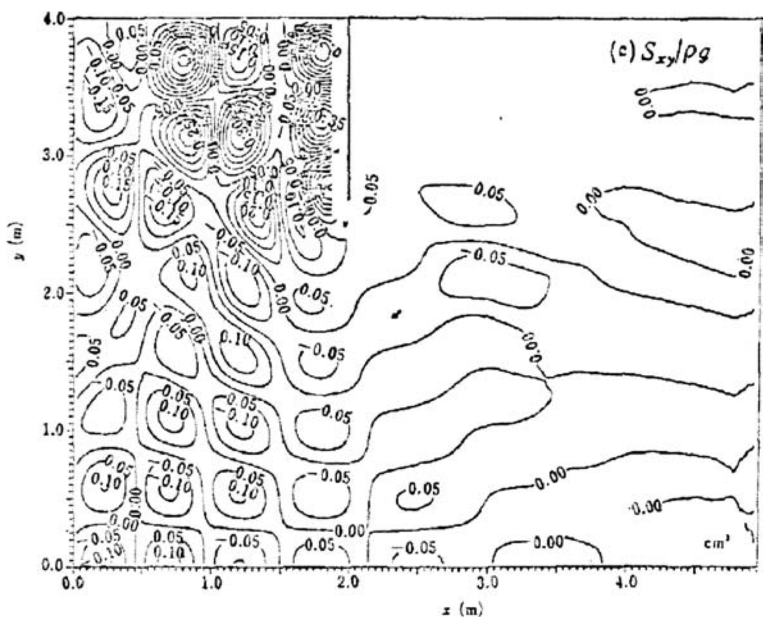

Fig. 7 S_{xy} from Watanabe & Maruyama (1986) solution

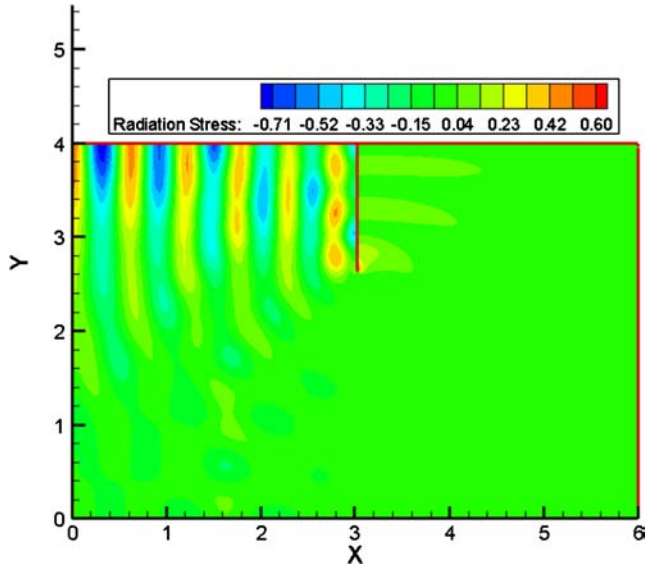

Fig. 8 S_{yy} from the authors' radiation stress model in N/m

published by Watanabe and Maruyama (1986) as illustrated in Figs. 6 – 11

S_{xy} and S_{yy} from the authors' model in Figs. 6 and 8 are very similar to those of Watanabe and Maruyama (1986) in Figs. 7 and 9. Watanabe and Maruyama (1986) mention on their figures that their values of radiation stress are divided by ρg although when compared with the authors' results (N/m) this does not appear to be the case. There appears to be some difference in the calculated values of S_{xx} as shown in Figs. 10 and 11. However, shorewards of the breakwater the radiation stress values are in very good agreement. This region is by far the most important for the development of set-up/set-down and wave-driven currents. It is also worth noting that although the trend appears different seaward of the breakwater in Figs. 10 and 11 the magnitude of the authors' values and those of Watanabe and Maruyama (1986) are still very similar in this region. The comparison illustrated in Figs. 3–5 above combined with the promising results of Figs. 6–9 and the set-up/set-down and current results described in Results Section 3 tend to give confidence in the radiation stress values calculated by the developed model.

5.4 Results (3a)–One-dimensional model compared to Liu and Mei's (1976) solution for a waves approaching a uniform beach

The authors' one-dimensional model, described in detail above, was tested for the case of a 10 s wave of 0.5 m amplitude approaching a beach at an angle of 0° . The slope of the beach was one in 50. The ϕ values for this model were calculated analytically. Liu and Mei (1976) use the same wave and beach slope for a model incorporating a detached breakwater as shown in Figs. 13–16. The results of the authors' one-dimensional model, shown in Fig. 12, without a breakwater can be compared with regions of the Liu and Mei (1976) solution that are remote from the shadow zone created by the breakwater in Fig. 15. The results compare quite well. The set-up in the authors' model is approximately 0.3 m at 10 m from the shoreline. From Fig. 15 it can be seen that in the same region the set-up of the the Liu and Mei (1976) model is also 0.3 m. Fig. 15 also shows the set-down to be 0.04 m at 125 m from the shoreline (in the region remote from the breakwater). The results of the authors' one-dimensional show a set-down value of approximately 0.04 m in this region also.

Fig. 9 S_{yy} from Watanabe & Maruyama (1986) solution

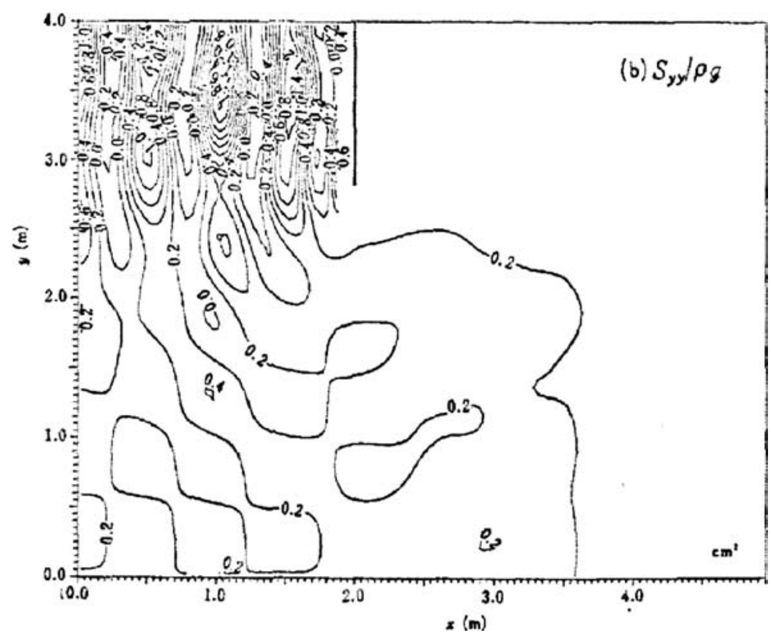

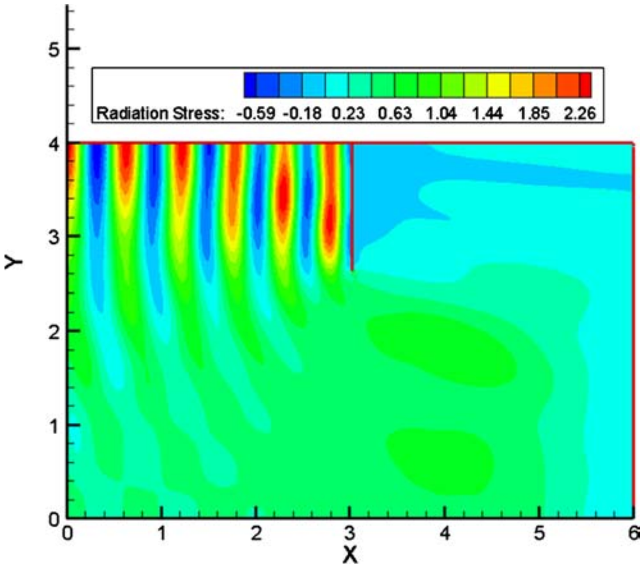

Fig. 10 S_{xx} from the authors' radiation stress model in N/m

5.5 Results (3b)–Two-dimensional model compared to Liu and Mei's (1976) solution for waves approaching a detached breakwater

More complex models are also examined. In each of these cases, the authors are grateful for the use of the elliptic extended mild-slope wave model of Clyne and Mullarkey (2004) which provides the ϕ values to be used in the authors' set-up/set-down and current model. The particular case examined is breaking-wave generated currents in the vicinity of a detached breakwater from Liu and Mei (1976). The waves approach a detached breakwater on a sloping beach. In the first case, the waves approach the beach straight in, and in the second case the waves approach at 60° (deep water) angle. The wave properties in each case are for a 10 s wave with an amplitude of 0.5 m. The beach slope is one in 50 and the detached breakwater is situated 350 m offshore.

Figures 13 and 14 show the authors' results obtained for the wave approaching straight in. The set-up and set-down is very apparent in the regions to either side of the breakwater and as expected in the shadow zone there is very little activity. Fig. 14 shows the vortex created by the sudden change in water elevations. The flow in this vortex is driven almost exclusively by hydrostatic forces because these outweigh the effects of radiation stress in this area. Figures 15 and 16 show the set-up/set-down and a streamline result obtained by Liu and Mei (1976) for the same case. The results of the authors' model and the Liu and Mei (1976) results are close for this case. The set-up in the authors' model appears a bit lower, but the set-down is almost identical to that of Liu and Mei (1976). It is expected that this difference could be due to a slight inaccuracy in the ϕ results obtained from the elliptic extended mild slope wave model in regions of very shallow water. This is further confirmed by the fact that the one-dimensional model using the same equations but analytical ϕ values gives a set-up exactly in line with Liu and Mei (1976). It is possible that an iterative scheme in the two-dimensional model that would increase the depth in line with set-up between calculations could help to reduce this inaccuracy.

Figures 17 and 18 show the results obtained for the wave approaching at a 60° (deep water) angle. The set-up and set-down results are similar to the straight in results but are skewed due to the different shadow zone caused by the approach angle of the waves. As detailed above, the authors' model provides an almost identical

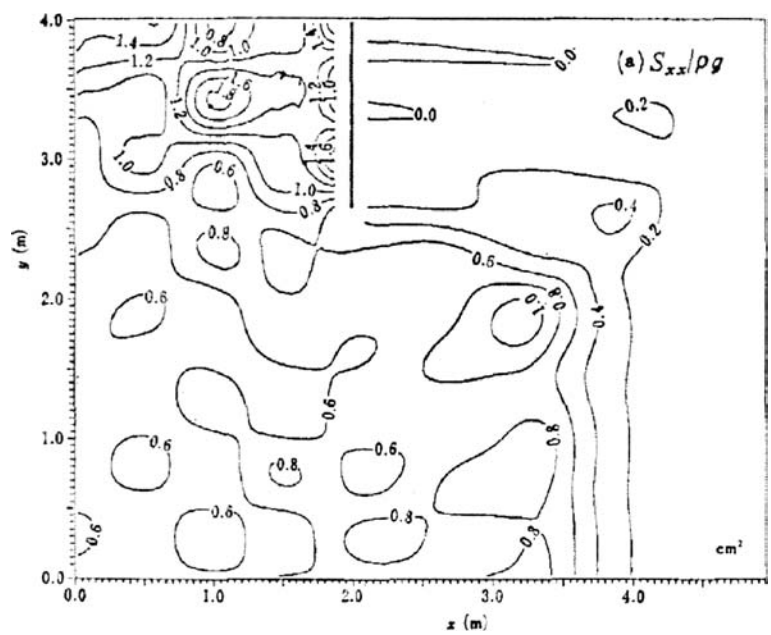

Fig. 11 S_{xx} from Watanabe & Maruyama (1986) solution

set-down and a slightly lower set-up than the Liu and Mei (1976) solution; it is expected that the reason is the same as surmised above. Figure 18 shows the reduction and concentration in current occurring at the edge of the shadow zone. This behaviour is also very obvious in Fig. 20, the Liu and Mei (1976) solution, along with a slight vortex effect that is somewhat apparent in the authors' results also.

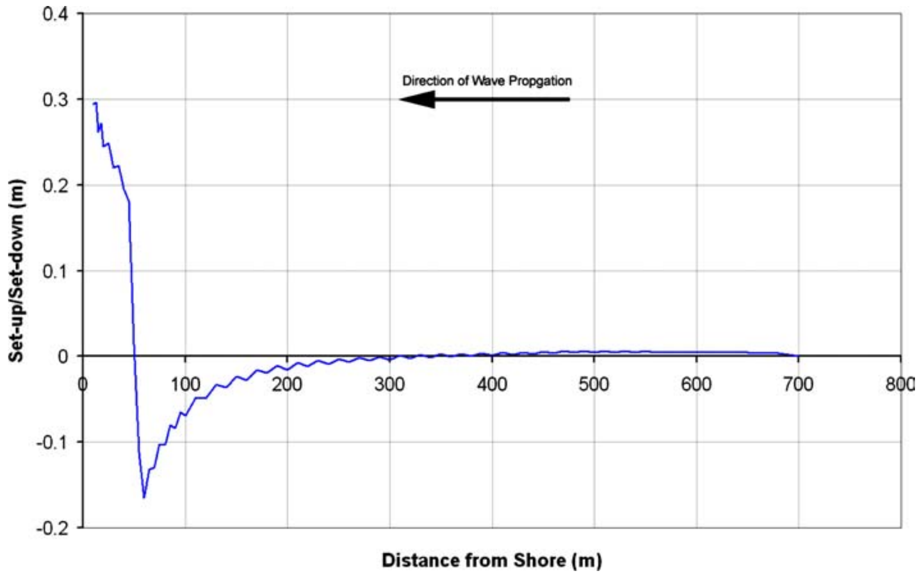

Fig. 12 Set-up/set-down from authors' one-dimensional model

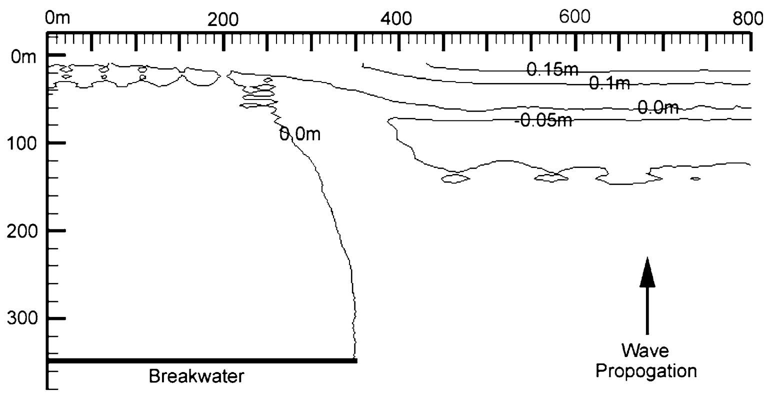

Fig. 13 Set-up/set-down for wave approaching breakwater straight in

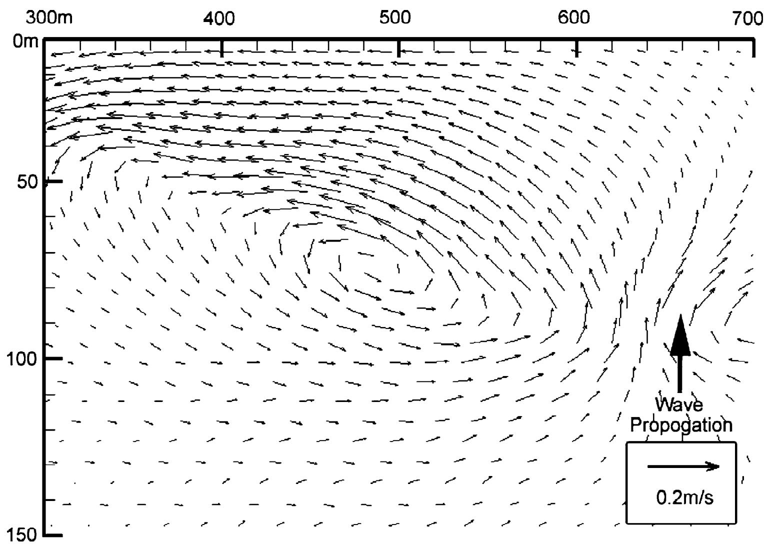

Fig. 14 Velocity plot for wave approaching breakwater straight in

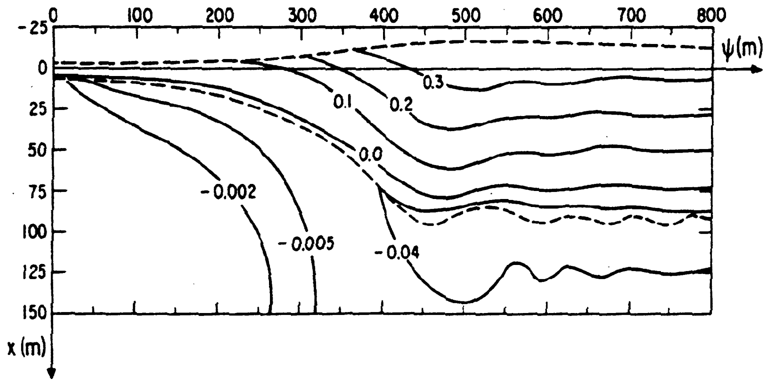

Fig. 15 Contour plot of set-up/set-down for wave approaching breakwater straight in (from Liu and Mei - 1976)

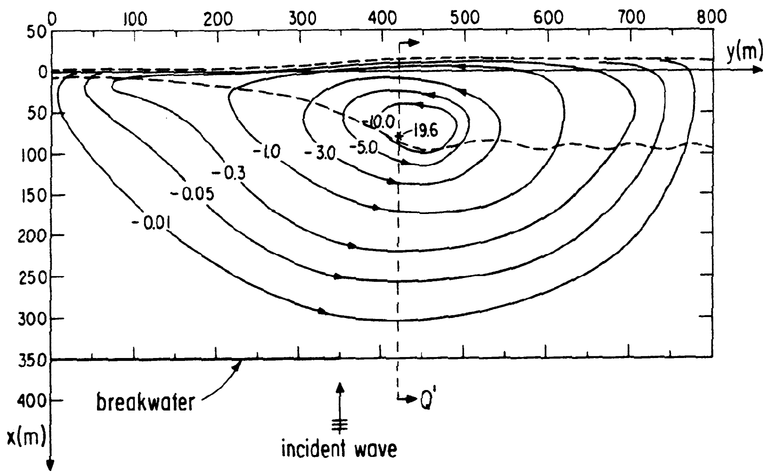

Fig. 16 Streamline plot for wave approaching breakwater straight in (from Liu and Mei 1976)

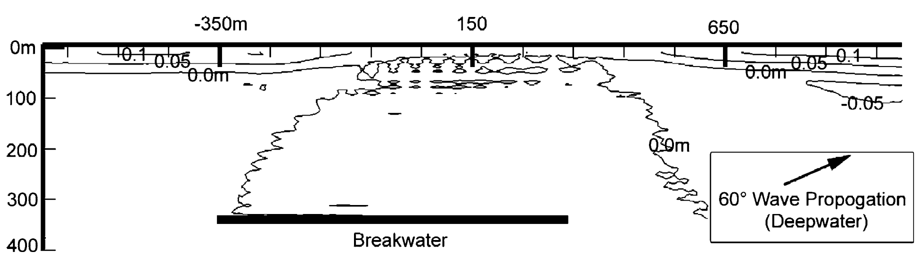

Fig. 17 Set-up/set-down for wave approaching breakwater at a 60° angle

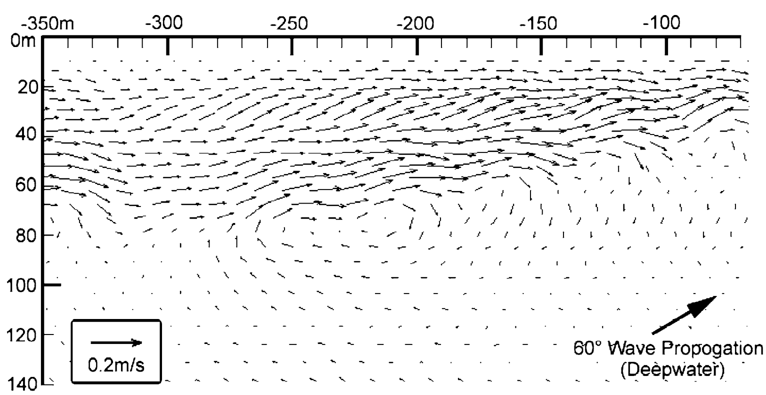

Fig. 18 Velocity plot for wave approaching breakwater at a 60° angle

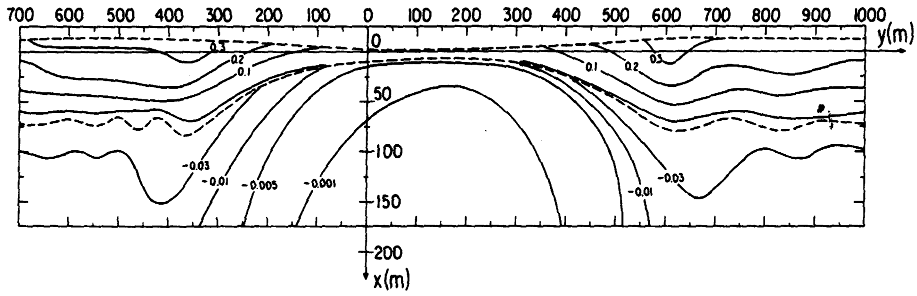

Fig. 19 Contour plot of set-up/set-down for wave approaching breakwater at a 60° angle (from Liu and Mei 1976)

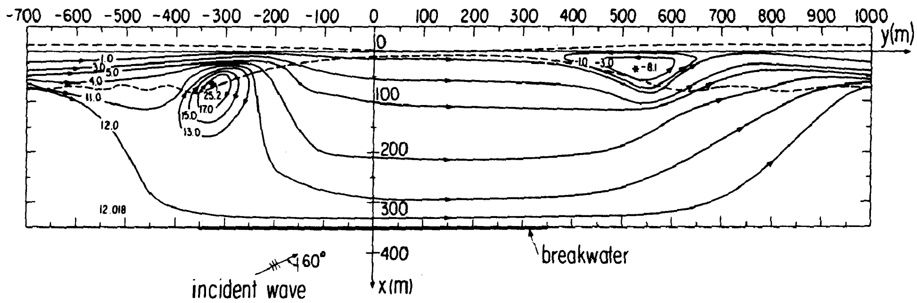

Fig. 20 Streamline plot for wave approaching breakwater at a 60° angle (from Liu and Mei 1976)

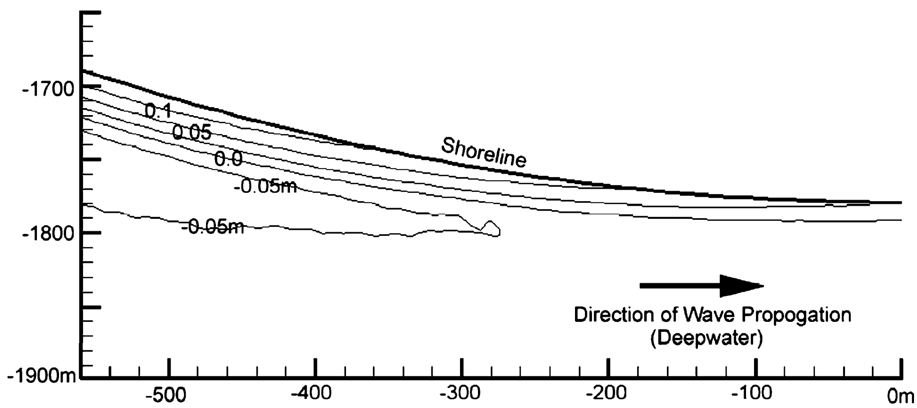

Fig. 21 Set-up/set-down for wave approaching a conical island

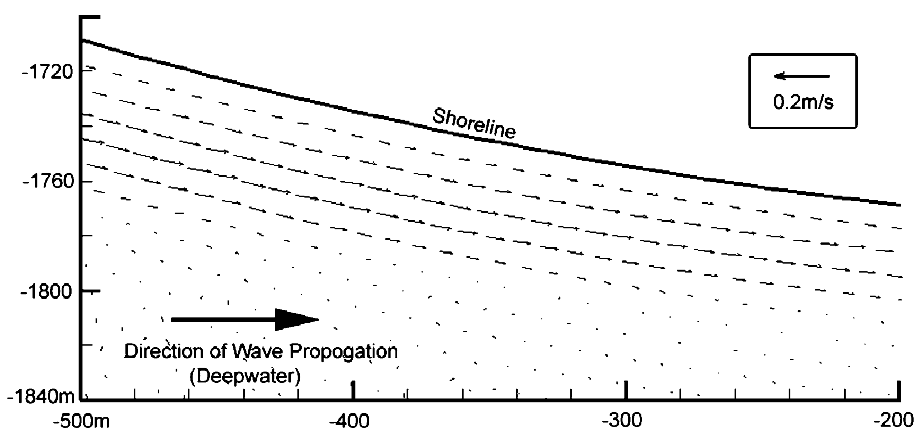

Fig. 22 Velocity plot for wave approaching a conical island

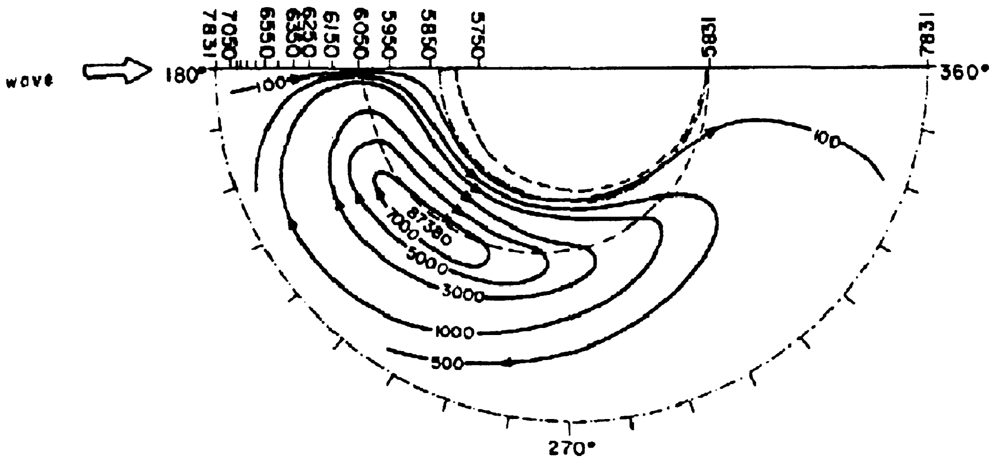

Fig. 23 Streamline plot for wave approaching a conical island (from Mei and Angelides 1976)

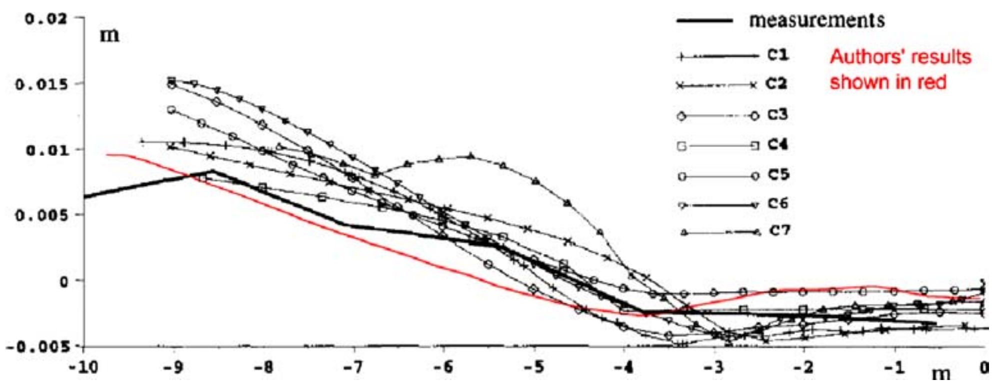

Fig. 24 Set-up/Set-down for different wave-driven current models (from Péchon et al. 1997)

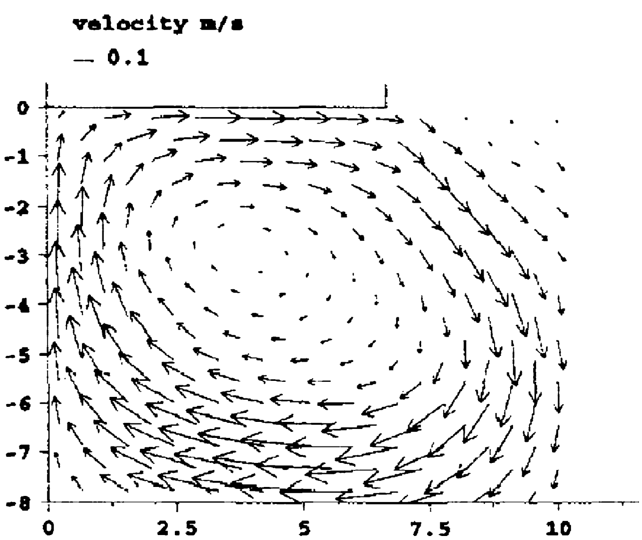

Fig. 25 Vortex generated behind a breakwater by MIKE 21 model (from Péchon et al. 1997)

5.6 Results (3c)–Two-dimensional model compared to Mei and Angelides' (1976) solution

Mei and Angelides (1976) provide results for waves approaching a conical island. The conical island has a radius of approximately 1,780 m. The beach slopes at one in 20 until the water depth reaches 30.5 m at which point, the sea bed becomes level. Waves approach the island with a period of 10 s and an amplitude of approximately 0.91 m. The results of the authors' model are shown in Figs. 19 and 20. No set-up/set-down values are given by Mei and Angelides (1976) but the streamline results are shown in Fig. 23. Figure 21 shows set-up/set-down results for one of the more interesting sections of the model, in this region the set-up and set-down are decreasing in magnitude due to the shape of the shoreline with respect to the direction of wave propogation. In Figs. 21 and 22, the centre of the island is located at the 0,0 coordinate. The streamline plot of longshore current shown by Mei and Angelides (1976) appears to compare well with the authors' results shown in Fig. 22.

5.7 Results (3d)–Two-dimensional model compared to Péchon et al (1997) solution for a half detached breakwater

Péchon et al (1997) examine seven different wave-driven current models for the case of a wave tank with a half detached breakwater as described in Results (1). The developed model was compared with the results of these

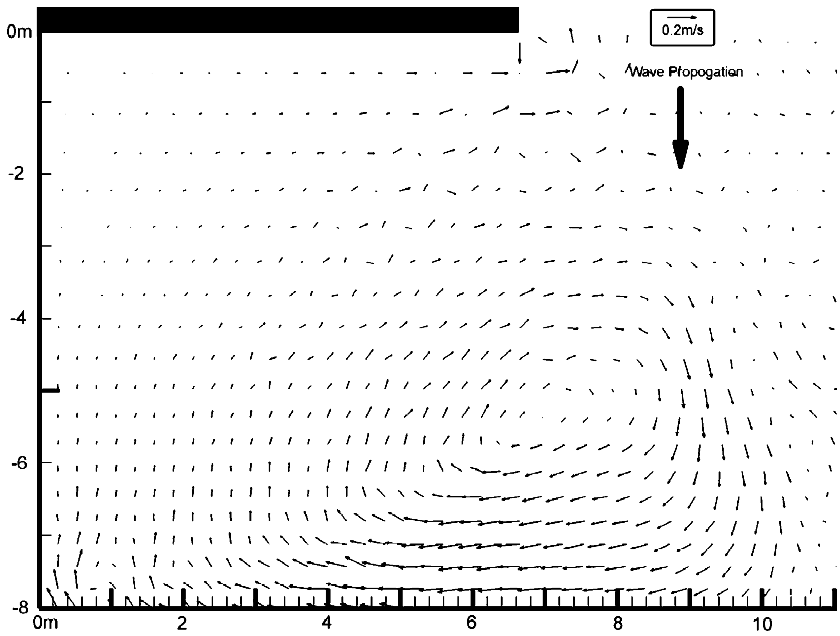

Fig. 26 Vortex generated behind a breakwater using developed model

models. Fig. 24 shows the set-up/set-down results obtained from the models and obtained experimentally. Most of the models tend to over predict the set-up whereas the authors' model slightly under predicts the set-up. The results of the authors model are quite close to the measured values and hence give a good level of confidence in the model.

Figure 25 shows the computed velocity field behind the breakwater for the MIKE 21 model. The field computed by the authors' model is shown in Fig. 26. The centre of the vortex in the authors' model is to the right of that computed by the MIKE 21 model. This could be due to the slightly lower set-up values occurring in the developed model. The overall shape and behaviour of the vortex appears similar to that of MIKE 21. It is worth noting that this situation is quite similar to that of the detached breakwater shown in Results (3b) where the position of the vortex predicted by the authors' model was almost identical to that predicted by the Liu and Mei (1976) solution. Melo et al. (1999) also examine the velocity field for this case. The results are very similar to those published by Péchon et al. (1997). It is also apparent from Figs. 25 and 26 that the magnitude of the velocities in the developed model are very similar to those occurring in the MIKE 21 model.

6 Conclusion

The developed model efficiently calculates radiation stress values from the velocity potential ϕ, and using these radiation stress values accurately calculates the set-up/set-down and currents that occur in the surf zone. For the one-dimensional case the contribution of the onshore S_{xx} component of radiation stress leads to the change in mean sea level (set-up/set-down) and the shear S_{xy} component produces currents. Inclusion of bottom friction is necessary in order for the model to converge. The authors' model compares well with published results. It includes non-linear convective acceleration and bottom friction terms and incorporates the behaviour of diffracted waves because of the elliptic equation used in the ϕ model. The investigation of wave-current interaction (Doppler effect) and turbulent diffusion are the next steps for the development of this model.

References

Berkhoff JCW (1976) Mathematical models for simple harmonic linear water waves–wave diffraction and refraction. Delft Hydraulics Laboratory, Delft University of Technology, p. 111

Booij N (1981) Gravity waves on water with non-uniform depth and current. Delft Hydraulics Laboratory, Delft University of Technology, 127p

Clyne M, Mullarkey T (2003) Wave models with energy dissipation using two representations of potential. Proceedings of the 13th International offshore and polar engineering conference pp 286–293

Clyne M, Mullarkey T (2004) Parabolic absorbing and radiating boundary conditions with diffraction and wave breaking. Proceedings of the 14th International offshore and polar engineering conference, pp 594–601

Liu PLF, Mei CC (1976) Water motion on a beach in the presence of a breakwater 2. Mean currents. J Geophys Res–Oceans and Atmosphere 81:3085–3094. Figures reprinted with permission from American Geophysical Union (AGU)

Longuet-Higgins MS, Stewart RW (1962) Radiation stresses and mass transport in gravity waves with applications to surf-beats. J Fluid Mech 13:481–504

Longuet-Higgins MS, Stewart RW (1964) Radiation stresses in water waves; a physical discussion with applications. Deep Sea Res 11:529–562

Maa JP-Y, Hsu T-W, Lee D-Y (2002) The RIDE model: an enhanced computer program for wave transformation. Ocean Engineering 29:1441–1458

Mei CC (1994) The applied dynamics of ocean surface waves. World Scientific Publishing Co. Pte. Ltd. Chapt. 10

Mei CC, Angelides D (1976) Longshore currents around a conical island. Coastal Engineering 1:31–42. Figures reprinted with permission from Elsevier

Melo E, Le Poole S, Martins RP (1999) Modelling wave-driven currents in the surf-zone. Resumos do 3o Seminário sobre Ondas e Marés/2o Simpósio sobre Engenharia Oceânica, IE-APM, Arraial do Cabo, RJ

Péchon P, Rivero F, Johnson H, Chesher T, O'Connor B, Tanguy J-M, Karambas T, Mory M, Hamm L (1997) Intercomparison of wave-driven current models. Coastal Engineering 31:199–215. Figures reprinted with permission from Elsevier

Pinder GF, Gray WG (1977) Finite element simulation is surface and subsurface hydrology. Academic Press Inc., London. Chapt. 8. Figures reprinted with permission from Elsevier

Watanabe A, Maruyama K (1986) Numerical modelling of near-shore wave field under combined refraction, diffraction and breaking. Coastal Engineering in Japan, Vol. 29. p. 19–39. Figures reprinted with permission from World Scientific Publishing Co. Pte. Ltd